1. Title page

i. Title: Seasonal changes in isoprene emission and deposition in central Amazonia

ii. Running head: a shortened title with no more than 45 characters, including spaces

iii. *Eliane G. Alves (1), Julio Tóta (2), Andrew Turnipseed (3), José Oscar W. Vega Bustillos (4), Raoni Aquino Santana (2), Paula Regina Corain Lopes (4), Glauber Guimarães Cirino (1), Julia Valentim Tavares (5), Aline Lopes (5), Bruce Nelson (5), Diogo Rosa (5), Dalton Vale (5), Rodrigo de Souza (6), Dasa Gu (7), Trissevgeni Stavrakou (8), David Adams (9), Jin Wu (10), Scott Saleska (11), Cleo Dias-Junior (12), Ana Maria Yãnez-Serrano (13), Jürgen Kesselmeier (14), Thomas Karl (15), Antonio Manzi (16), Alex Guenther (7).*

iv. (1) Environment Dynamics Department, National Institute for Amazonian Research (INPA), Av. André Araújo 2936, CEP 69067-375, Manaus-AM, Brazil.

(2) Institute of Engineering and Geoscience, Federal University of West Para (UFOPA), Rua Vera Paz s/n, CEP 68035-110, Santarem-PA, Brazil.

(3) Atmospheric Chemistry Division, National Center for Atmospheric Research (NCAR), 3450 Mitchell Lane, Boulder, CO 80301, U.S.A.

(4) Chemistry and Environment Center, National Institute for Energetic and Nuclear Research (IPEN), Av. Lineu Prestes 2242, CEP 05508-000, São Paulo-SP, Brazil.

(5) Ecology Department, National Institute for Amazon Research (INPA), Av. André Araújo 2936, CEP 69067-375, Manaus-AM, Brazil.

(6) Meteorology Department, State University of Amazonas (UEA), Av. Darcy Vargas 1200, CEP 69050-020, Manaus-AM, Brazil.

(7) Department of Earth System Science, University of California, Irvine, CA 92697, USA.

(8) Belgian Institute for Space Aeronomy, Avenue Circulaire 3, 1180 Uccle, Brussels, Belgium.

(9) Centro de Ciencias de la Atmósfera, Universidad Nacional Autónoma de México, Av. Universidad 3000, 04510, Mexico city, Federal District, Mexico.
(10) Terrestrial Ecosystem Science and Technology, Brookhaven National Laboratory, Brookhaven Ave, Upton, NY 11973, USA.
(11) Ecology and Evolutionary Biology Department, University of Arizona, Cheery Avenue and University Boulevard, Tucson, AZ 85721, USA.
(12) Federal Institute of Para, Rua da Escola Agrícola, CEP 68600-00, Bragança, Pará, Brazil
(13) Institute of Ecosystem Physiology, University of Freiburg, Georges-Koehler-Allee 53, 79110 Freiburg, Germany.
(14) Biogeochemistry Department, Max Planck Institute for Chemistry, 55128, Mainz, Germany
(15) Institute of Meteorology and Geophysics, University of Innsbruck, Innrain 52, 6020, Innsbruck, Austria.
(16) National Institute for Spatial Research, Center of Weather Forecasting and Climate Studies, Rod. Presidente Dutra, km 40, Cachoeira Paulista-SP, Brazil.
v. corresponding author: +55 92 3643 3238; elianegomes.alves@gmail.com
vi. Keywords: biogenic volatile organic compounds, isoprene, tropical rainforest, leaf demography, leaf phenology, seasonality.
vii. Primary Research Article

2. Abstract

Isoprene fluxes vary seasonally with changes in environmental factors as light and temperature, and biological factors as leaf phenology. But, our understanding of isoprene seasonal dependency to these factors is still limited in Amazonia. It has been indicated that the dry season shows higher emissions than the wet season, because there is more light available and higher temperature. Also, leaf phenology was recently suggested to drive ecosystem isoprene emissions, but local seasonal observations were scarce or not available. Here, we present canopy isoprene flux measured in two sites of primary rainforest in central Amazonia and compare to changes in light, temperature, and leaf phenology. The highest emissions were during the dry and dry-to-wet transition seasons, and the wet and the wet-to-dry transition seasons revealed net deposition for one site. Leaf phenology, referred as changes in observed mature Leaf Area Index, was the most correlated factor and explained up to 59% of seasonal isoprene emissions. Attempting to represent this with modeling, the MEGAN 2.1 leaf age algorithm was driven by inputs resulted from a leaf demography-ontogeny model that uses leaf flushing observed in the fields. However, model emissions were overestimated and did not capture the seasonal behavior observed. Using the leaf phenology from the field as inputs for the leaf age algorithm of MEGAN 2.1, improved estimates of the proportion of leaves in different leaf age categories for each site, but did not change the relative isoprene emission capacity used for each age class. This study hightlights the importance of accounting for differential isoprene emission capacity across canopy leaf age classes and of identifying the forest adaptive mechanisms that underly seasonal variation of emission, and potentially deposition, of isoprene in Amazonia.

3. Introduction

Isoprene is considered the dominant emission from many landscapes and has the largest contribution to total global vegetation Biogenic Volatile Organic Compound (BVOC) emission, with estimates of about 400─600 Tg C y^{-1} (see Table 1 of Arneth *et al.*, 2008). The plant functional roles of isoprene production and emission are still in open debate, but some hypotheses have been proposed: isoprene could be a thermal protectant for plants against high temperatures (Sharkey & Singsaas, 1995; Loreto & Velikova, 2001); this compound may quench oxidative damages (Loreto *et al.*, 2001; Vickers *et al.*, 2009); it could serve as a metabolic mechanism to deal with the overflow of carbon or photosynthetic energy (Logan *et al.*, 2000; Rosenstiel *et al.*, 2004; Sanadze, 2004); it could play a role to deter herbivory (Laothawornkitkul *et al.*, 2008); and it could promote flowering in adjacent plants (Terry *et al.*, 1995). Once in the atmosphere, isoprene has implications in the chemical and physical processes due to its reactivity, influences on the atmospheric oxidative capacity, and has potential to form secondary organic aerosols (Claeys *et al.*, 2004). Moreover, CO_2 is believed to be the fate of almost half of the carbon released in form of BVOCs (Goldstein & Galbally, 2007) and, as isoprene is the most emitted, this compound might play important role on carbon balance.

Tropical forests contribute almost half of the estimated global annual isoprene emission, ranging from about 220 to 340 Tg according to the estimates of the Model of Emissions of Gases and Aerosols from Nature (MEGAN) (Guenther *et al.*, 2006). There are large uncertainties associated with these estimates, particularly because of differences in the model-driving variables (Guenther *et al.*, 2006), and because detailed information from observational studies in remote tropical forests is still scarce. Yet, some studies have used concentration columns of formaldehyde (HCHO) (one isoprene oxidation product) observed by satellites to constrain the isoprene fluxes and to possibly improve the bottom-up

inventories of isoprene (Stavrakou *et al.*, 2014). This approach indicated the seasonal variation in isoprene emission over the South America (Barkley *et al.*, 2008, 2013), and particularly over the Amazonian rainforest (Barkley *et al.*, 2009).

Despite remote sensing observations have shown isoprene seasonal variation, only a few *in situ* observational investigations have been carried out to verify this seasonality in the Amazonian rainforest (Andreae et al., 2002; Kesselmeier et al., 2002; Kuhn et al., 2004a; Yañez-Serrano et al., 2015; Alves et al., 2016). Some of those studies have suggested that the primary drivers of the isoprene seasonality are environmental factors such as solar radiation and temperature. During the dry season more solar radiation is available at the surface and, consequently, temperature is higher than other year periods. As isoprene is light and temperature dependent, seasonal changes in these two factors influence variation in emissions. When only light and temperature are considered, MEGAN is shown as a satisfactory tool to predict short-term changes in isoprene emissions in Amazonia and other tropical forests (Karl *et al.*, 2004, 2007; Misztal *et al.*, 2011) . Nevertheless, when long-term changes are taking place, other factors might be acting together, some of them still unknown, which add uncertainties to the predictions of isoprene seasonal emissions.

Recently, canopy phenology was indicated as the primary cause of seasonal changes of photosynthesis in Amazonian ecosystems (Wu *et al.*, 2016). Given the facts that photosynthesis provides substrates and energy for isoprene production and that isoprene is not stored within leaves, canopy phenology could therefore be an important driver of seasonal changes in ecosystem isoprene emissions, as already been suggested (Alves et al., 2014; 2016). However, even though these factors – solar radiation, temperature and leaf phenology – have been pointed out as important drivers of isoprene seasonal emissions, the controls on isoprene seasonality are still poorly understood and unsatisfactorily represented in biogeochemical models due to the lack of observations in Amazonia. In the context of

climate changes, understanding how isoprene emissions, and potentially deposition, change seasonally and behave in anomalous years, when there is extreme conditions that are expected to be more frequent in the future, would improve predictions on which way isoprene acts on the atmospheric chemistry and carbon balance.

Here, we present observations of seasonal variations of isoprene fluxes, solar radiation, air temperature and canopy phenology of two experimental sites of primary rainforest in central Amazonia. We ask the following questions: (i) what is the seasonal pattern of isoprene fluxes?; (ii) how seasonal isoprene fluxes can be explained by variations in solar radiation, temperature and leaf phenology?; and (iii) how leaf phenology observed in field can help on improving model estimates of isoprene seasonal emissions? To address these questions we correlated ground-based isoprene flux measurements to environmental factors (light and temperature) and to a biological factor (leaf phenology). We compared seasonal ground-based isoprene flux measurements to seasonal satellite-derived isoprene flux. Lastly, we did two runs with the MEGAN 2.1 to estimate isoprene fluxes: (1) in default mode and (2) with the leaf age algorithm parameterized with leaf phenology observed in the field.

4. Material and methods

Site Descriptions

a. Cuieiras Biological Reserve - K34 tower (ZF2)

Isoprene fluxes were measured at the K34 tower (2°36' 32.67" S, 60° 12' 33.48" W) on a plateau of the Cuieiras Biological Reserve, a primary rainforest reserve located approximately 60 km northwest of Manaus city, in the central Amazonian Basin, in Amazonas, Brazil (Fig. 1). The K34 tower has been widely utilized for over 15 years for a

147 range of meteorological studies, including energy and trace gases fluxes (de Araújo *et al.*,
148 2010; Tóta *et al.*, 2012) and also tropospheric variables such as precipitable water vapor
149 (Adams *et al.*, 2011). This reserve has an area of about 230 km² and belongs to the National
150 Institute for Amazonian Research (INPA). A maximum altitude of 120 m characterizes the
151 topography. The site is characterized by 31 % of plateau, 26 % slope and 43 % valley (Rennó
152 *et al.*, 2008). Soils are well-drained Oxisols and Ultisols on the plateau and slopes,
153 respectively, and poorly drained Spodosols in the valleys (Luizao *et al.*, 2004). The
154 vegetation in this area is considered mature, *terra firme* rainforest, with a leaf area index of
155 4.7 (Malhi *et al.*, 2009), and with typical canopy height of 30 m with variation (20-45 m)
156 throughout the reserve. The diversity of tree species is greater than 200 species ha^{-1} (Oliveira
157 *et al.*, 2008). Annual precipitation is about 2500 mm and dominated by deep atmospheric
158 convection and associated stratiform precipitation, with the wetter season from December to
159 May and the drier season from August to September, when the monthly cumulative
160 precipitation can be less than 100 mm per month (Machado *et al.*, 2004; Adams *et al.*, 2013) .
161 Average air temperature ranges between 24 °C (in April) and 27 °C (in September) (Alves *et*
162 *al.*, 2016). Soil moisture shows a small reduction (~ 10%) of water availability during the dry
163 season compared to the wet season (Cuartas *et al.*, 2012). Measurements, in this site, were
164 during intensive campaigns from June 2013 to December 2013. The period from June to July
165 represents the wet-to-dry transition season, August to September the dry season, October
166 through November the dry-to-wet transition season, and December the beginning of wet
167 season.

168 *b. Amazon Tall Tower Observatory (ATTO) – INSTANT tower*

169 Isoprene gradient fluxes were measured in the ATTO site, which is located in central
170 Amazonia, 150 km northeast of Manaus in the Uatumã Sustainable Development Reserve
171 (USDR) (Fig. 1). The climate is tropical humid, with mean annual precipitation of 2376 mm

and mean annual temperature of 28 ºC (IBGE, 2012). The seasons are presumably similar to the Cuieiras Biological Reserve site due to the relative geographical proximity between both sites (~100 km). The most of air masses arriving at the site comes from northeast and has passed through 1500 km of undisturbed *terra firme* rainforest, with negligible intrusion of air masses from Manaus (Yáñez-Serrano *et al.*, 2015). The vegetation in this area is considered mature, *terra firme* rainforest, with a mean canopy height of 35 m. The 80 m tower (INSTANT tower; 02º 08' 38.8'' S, 58º 59' 59.5'' W) is located approximately 12 km northeast of the Uatumã River, where *terra firme* forest is predominant on plateaus at a maximum altitude of approximately 130 m a.s.l. (Andreae *et al.*, 2015). More details of this experimental site can be found in Andreae et al. (2015). Isoprene gradient flux measurements occurred during intensive field campaigns from November 2012 to October 2015, taking into account the dry, the wet, and the transition seasons (Table 1).

Isoprene flux (K34 site) – Relaxed Eddy Accumulation system

Measurements of isoprene fluxes were carried out using a Relaxed Eddy Accumulation system (REA) developed by the National Center for Atmospheric Research (NCAR) (REA, NCAR/BEACHON Cassette Sampler, S/N #:1001). This REA system was installed at a height of 48 m of the K34 tower (approximately 20 m above the mean canopy height). The fundamental basis of this technique is to segregate the sample flow according to the vertical wind velocity measured by the sonic anemometer over the flux-averaging period (30 min). The basic equation to derive isoprene fluxes (F) from the REA system over this period was:

$$F = \overline{w'c'} = b\sigma_w(\overline{c_{up}} - \overline{c_{down}}) \quad (1)$$

where b is an empirical proportionality coefficient (described below), σ_w is the standard deviation of w, and $\overline{c_{up}}$ and $\overline{c_{down}}$ are the average of the isoprene concentrations in the up and down reservoirs, respectively (Bowling *et al.*, 1998). The b-coefficient was calculated from the sonic temperature and heat flux by re-arranging the same equation, assuming scalar similarity (Monin-Obukhov Similarity Theory):

$$b = \frac{\overline{w'T'}}{\sigma_w(T_{up} - T_{down})} \quad (2)$$

The REA requires two initial data points at the beginning of each flux averaging period to be able to segregate the sample flow: (1) a mean vertical wind velocity, $\overline{w}$ and (2) σ_w. The $\overline{w}$ is needed to determine the direction of the instantaneous vertical wind velocity ($w' = w(t) - \overline{w}$) and σ_w is required to calculate a "deadband". A deadband was a range of small w' values, centered on $\overline{w}$, over which the air was sampled through the "neutral" line. The deadband was $\pm 0.6\sigma_w$. The use of a deadband is advisable, because this increases the differences in the measured concentrations ($\overline{c_{up}} - \overline{c_{down}}$), which allows the sampling of only larger eddies (with larger concentration fluctuations) into the up/down reservoirs, reducing restrictions on the analytical technique used. The b-coefficient was also computed (from eq. 2) using the same deadband. For this study, b-coefficient ranged 0.3-0.6.

The basic components of the REA are (1) the Main REA box containing the adsorbent cartridges (stainless steel tubes filled with Tenax TA and Carbograph 5TD adsorbents) for reservoirs up/down/neutral, microcontroller, battery, data logger, selection valves and mass flow controller (200 ml min^{-1}) (MKS Instruments Inc., Model M100B01852CS1BV) and (2) a Sonic Anemometer (RM Young, Model 81000VRE) for fast wind velocity measurements.

According to Arnts et al. (2013), there are three main sources of errors that give uncertainties to the REA technique – time lag, non-constant flow achievement, and chemical

losses. Since air sample segregation into the respective reservoirs – up, down, and neutral – should be performed without cross-contamination from the other direction, the time spent to measurements of wind velocity and direction, and then to compute and execute the respective command, needs to be fast enough to avoid time lag. To reduce this problem, the REA sampling was carried out with two tubing lines for up (+w') and down (-w') and one tubing line for neutral sampling air ($\pm 0.6\sigma_w$ - deadband), each consisting of about 1.5 m long tubes (polytetrafluoroethylene, PTFE). Too long distances (> 2m) likely cause errors in the measured flows when valves are switching rapidly. Each inlet valve at the main REA box prevented air from entering the inactive tube (up- in case down sampling (-w') and down - in case up sampling (+w'), and both up and down in the case deadband), which otherwise would compromise the concentration differences between up and down reservoirs and, consequently, the flux calculation. The sonic anemometer took samples at 10 Hz. A data logger recorded the sonic anemometer data and a microcontroller accomplished the data acquisition and the valve triggering. The switching valve was based on the last flux-averaging period (30 min) of $\overline{w}$ and σ_w, the valves being activated according to the threshold condition ($\pm 0.6\sigma_w$, in the case of threshold condition, the valve of the neutral inlet, deadband, was activated). After 30 min of sampling, the data logger stored all the necessary wind and temperature information to compute the flux according to equation (1).

This REA system with three couples of valves (upstream and downstream valves for up, down and neutral reservoirs) joined with a constant flow rate sampling (air samples were drawn by a pump and controlled by a mass flow controller at a rate of 200 ml min^{-1}) reduced problems with non equivalent pressure differential across the valve inlet(s) and exit, which means that constant flow of sample can be achieved through right placement of three way valves, mass flow controller and pump with adsorbent tube accumulators, diminishing the second source of error proposed by Arnts *et al.* (2013). To avoid the third problem, chemical

losses, the inlets (up, down, and neutral) were installed at the sonic anemometer height (48 m) with a filter for ozone and particle matter (Pall Corporation, Glass Fiber Acrodisc), and then connected to the Main REA box containing the adsorbent cartridges for the respective reservoirs up/down/neutral.

The mass accumulated in the adsorbent cartridges was determined from laboratory analysis. The isoprene concentrations were then determined using the amount of volume that was passed through each respective reservoir. This volume was measured by integration of the mass flow meter signal and stored within the REA data. All REA measurements were carried out during daytime from 9:00h to 16:30h, local time, in one intensive campaign per month. For each campaign, samples were collected during five or six consecutive days. All campaigns were carried out from June 2013 to December 2013.

Isoprene quantification (K34 tower site) - thermal desorption gas chromatography-flame ionization detection (TD-GC-FID)

Both up and down REA samples were collected by drawing 200 sccm of air through onto adsorbent tubes for 30 minutes. The adsorbent tubes were purchased commercially, filled with Tenax TA and Carbograph 5TD adsorbents (Markes International, UK). The tube samples were analyzed for isoprene with a thermal desorption system (TD) (Markes International, UK) interfaced to a gas chromatograph/flame ionization detector (GC-FID) (19091J-413 series, Agilent Technologies, USA). After loading a tube in the ULTRA Automatic Sampler (Model Ultra1, Markes International, UK), which was connected to the thermal desorption system, the collected samples were dried by purging for 5 minutes with 50 sccm of ultra-high purity helium (all flow vented out of the split vent) before being transferred (300ºC for 10 min with 50 sccm of ultra pure nitrogen) to the thermal desorption cold trap held at -10ºC (Unity Series1, Markes International, UK). During GC injection, the

trap was heated to 300°C for 3 min while back-flushing with carrier gas (helium) at a flow of 6.0 sccm directed to the column (Agilent HP-5 5% Phenyl Methyl Siloxane Capillary 30.0 m X 320 µm X 0.25 µm). The oven ramp temperature was programmed with an initial hold of 6 min at 27 °C followed by an increase to 85 °C at 6 °C min^{-1} followed by a hold at 200 °C for 6 min. The identification of isoprene from samples was confirmed by comparison of retention time with a solution of an authentic isoprene liquid standard in methanol (10 µg/ml in methanol, Sigma-Aldrich, USA). The GC-FID was calibrated to isoprene by injecting 0.0, 23, 35, and 47 nL of the gas standard onto separate tubes. The gas standard is 99.9% of 500 ppb of isoprene in nitrogen (Apel Gas Standard, USA) and was injected into separate tubes at 11 ml min^{-1}. The calibration curve (0.0, 23, 35, and 47 nL) was made thrice before the analysis of the sample tubes of each campaign, being the mean correlation coefficient equals to R^2=0.98. In addition, two standard tubes (with 35 nL of isoprene) were run at every 20 sample tubes to check the system sensitivity. The limit of detection of isoprene was equal to 48.4 ppt.

All tube samples were analyzed as described above with the exception of tube samples from June 2013 and July 2013. These tube samples were analyzed in a TD/GC-MS-FID system from the Atmospheric Chemistry Division of the NCAR. For this system, thermal desorption was carried out via a two-stage process, where the adsorbent cartridge was initially desorbed at 275^{o}C while passing a flow of ultra-high purity through using a commercial TD-autosampler (Model Ultra1, Markes International, UK). The sample was transferred via a heated line to a cold trap that was packed with Tenax-TA and cooled to 0^{o}C via peltier (Unity Series1, Markes International, UK). Once the entire sample was transferred to this intermediate trap, it is rapidly heated to 300^{o}C and injected onto the GC column (DB-5 column, Restek, 250 micron, etc.). The GC column was cryofocused to -30^{o}C and then temperature programmed up to 275^{o}C. After separation, the sample was split between the two

296 detectors (FID and Mass Spectrometer - MS). This system is calibrated daily by filling
297 adsorbent cartridges with a secondary standard consisting of isoprene and camphene. This
298 isoprene/camphene standard was calibrated relative to a NIST-certified butane/benzene gas
299 standard as well as a NIST-certified neohexane gas standard. The FID was used to quantitate
300 isoprene.

301 Isoprene was quantified in mg m^{-3}, then concentrations were subtracted from those found
302 in the blank tubes that have been connected to the cartridge cassete in the REA box during
303 the sampling, but without flow passing through. The resulted concentrations were used to
304 calculate isoprene flux (equation 1) in mg m^{-2} h^{-1}.

305

306 *Isoprene gradient flux (ATTO site) - Proton transfer reaction-mass spectrometer (PTR-MS)*
307 *and Inverse Lagrangian Transport model*

308 Measurements of isoprene gradient mixing ratios were carried out during intensive
309 campaigns from November 2012 to October 2015 (Table 1) at eight heights in and above the
310 canopy (0.05, 0.5, 4, 12, 24, 38, 53 and 79 m). Eight heated (50 ºC) and insulated inlets
311 (PTFE) were connected to a Proton Transfer Reaction – Mass Spectrometer (PTR-MS)
312 (Ionicon Analytic GmbH, Austria), which was housed in an air conditioned container 10 m
313 from the INSTANT tower. Before the sampled air was injected into the PTR-MS, inlets were
314 guided to a valve system switching every 2 min between the different heights, completing a
315 whole profile in 16 min. Mean total uncertainty of isoprene mixing ratios was 9.9 %, which is
316 within PTR-MS measurement uncertainty (~10%). More details of the experimental setup
317 and PTR-MS conditions and calibration can be obtained in Yãnez-Serrano et al. (2015).

318 Once isoprene mixing ratios were obtained, fluxes of isoprene were estimated using
319 the average daytime (12:00-15:00, LT) concentration vertical profile throughout the canopy

(from 4 to 38 m) and applying an inverse Lagrangian transport model (ILT) (Raupach, 1989; Nemitz et al., 2000; Karl et al., 2004; Karl et al., 2009, Alves et al., 2016). The source/sink distributions throughout the canopy were computed according to Eq. (3):

$$\vec{C} - C_{Ref} = \overleftrightarrow{D} . \vec{S} \quad (3)$$

where $\vec{C}$ is the concentration (g m^{-3}) vector for each level, C_{Ref} is the concentration (g m^{-3}) at reference height (38 m), $\overleftrightarrow{D}$ (m) is a dispersion matrix, and $\overrightarrow{S}$ (mg m^{-2} $h^{-1}$$layer^{-1}$) is the resulting source/sink vector. $\overleftrightarrow{D}$ is expressed as a function of Lagrangian timescale and profiles of the standard deviation of the vertical wind speed (σ_w), which was normalized to friction velocity (u_*). Integration over all source and sink terms ($\vec{S}$) yielded the canopy scale isoprenoid flux (mg m^{-2} h^{-1}). To parameterize $\overleftrightarrow{D}$, we use the Lagrangian timescale (Tl) parameterized according to Raupach (1989) and the vertical profile of the standard deviation of the vertical wind speed scaled to measured friction velocity. The normalized turbulence profile was taken from σ_w measurements inside and above the canopy and from friction velocity measured at 36 m. Both σ_w and u_* were averaged for each season-campaign using daytime data (12:00-15:00, LT) measured at the INSTANT tower, except for the two last campaigns, when measurements of σ_w and u_* were not fully available. For these two campaigns, averages of σ_w and u_* from another days of the same season were used. The calculation of $\overleftrightarrow{D}$ was based on the far- and near-field approach described by Raupach (1989). Taking the above conservative error assessment, which considered errors of turbulence (~26 %) added to errors of chemical identification (~10 %), uncertainties of the ILT method is estimated to be up to 36 % (see more details in section 1 of Supporting Information).

342 *Satellite-derived isoprene flux estimates*

343 Top-down isoprene emission estimates over the 0.5 degree region around the tower of
344 both sites – K34 and ATTO - were obtained by using a grid-based source inversion scheme
345 (Stavrakou *et al.*, 2009) constrained by formaldehyde (HCHO) columns, which is an
346 intermediate product of the isoprene degradation process (Stavrakou et al., 2014). HCHO was
347 measured by UV-visible sensors on the Ozone Monitoring Instrument (OMI)/Aura satellite
348 launched in 2004. The source inversion was performed using the global chemistry-transport
349 model IMAGESv2 (Intermediate Model of Annual and Global Evolution of Species) run at a
350 resolution of 2º × 2.5º and 40 vertical levels from the surface to the lower stratosphere
351 (Stavrakou *et al.*, 2014, 2015). The priori isoprene emission inventory was taken from
352 MEGAN-MOHYCAN-v2 (Stavrakou *et al.*, 2014,
353 http://tropo.aeronomie.be/models/isoprene.htm), and included updates regarding isoprene
354 emission rates from Asian tropical forests. IMAGESv2 used HCHO columns retrieved from
355 OMI sensor as top-down constraints and estimated the posterior biogenic isoprene emission.
356 Given that the OMI measurement overpass time is at early afternoon (13:30), and the mostly
357 delayed production of formaldehyde from isoprene oxidation, the top-down emission
358 estimate is dependent on the ability of MEGAN to simulate the diurnal shape of isoprene
359 emission and on the parameterization of chemical and physical processes affecting isoprene
360 and its degradation products in IMAGESv2. For this study, we use daily (24 hours) mean
361 satellite-derived isoprene emissions derived from January 2005 to December 2013 for the
362 K34 site, and from January 2012 to December 2014 for the ATTO site. More details can be
363 found in Stavrakou et al. (2009, 2014, 2015) and Bauwens et al. (2013).
364

365 *Leaf demography and phenology*

366 Upper canopy leaf phenology was monitored in both sites with a RGB Stardot (model
367 Netcam XL 3MP) camera installed on top of each tower - K34 (53 m) and INSTANT (81 m)
368 (ATTO) – with a respective resolution of 1024 x 768 and 2048 x 1536 pixels. Images were
369 logged every 15 s to a passively cooled FitPC2i microcomputer with heat-tolerant solid-state
370 drive. The whole system of data acquisition automatically rebooted after power outages.

371 For the K34 tower, the monitoring was based on the observation of leaf flushing
372 events of the upper crown surfaces of 63 living trees around the tower. The camera view was
373 south azimuth, perpendicular to the solar transit, centered on 32º of depression and pointing
374 out to an area of plateau. The images obtained by the camera covered approximately 66º
375 horizontally and 57º vertically, always monitoring tree crowns and excluding the sky. The
376 framework was fixed by monitoring the same 63 crowns over two years of observation (2012
377 – 2013). For the INSTANT tower (ATTO), 267 tree crowns were monitored. The camera
378 view was west (270º), monitoring the same trees, and not including the sky over two and a
379 half years (July 2013 – December 2015). Images have covered four hectares due to the 96º
380 wide-angle lens and due to the height of the camera installation (81 m). Image analysis of
381 both sites was based on the number of crowns that showed leaf flushing within one month.
382 More details of image analysis, greenness metric and detection of phenostages (leaf age
383 classes) over the seasons can be obtained in Lopes *et al.* (2016).

384 Once leaf age classes were accomplished for each site, Leaf Area Index (LAI) was
385 derived considering the total amount of leaves and fractionated into three leaf age classes –
386 young LAI, mature LAI and old LAI. To get the CAMERA-LAI derived data, leaf flushing
387 and litter fall were the inputs for the leaf demography-ontogeny model (Wu *et al.*, 2016). This
388 model was developed with observations of two sites in central Amazonia (Manaus – K34

tower, and Santarém – K67 tower), and more details about its settings and parameterizations can be obtained in Wu *et al.* (2016).

Modeled isoprene flux estimates - Model of Emissions of Gases and Aerosols from Nature (MEGAN 2.1)

Isoprene fluxes measured by REA (K34 site) and estimated by ILT (ATTO site) were compared with those estimated by the Model of Emissions of Gases and Aerosols from Nature (MEGAN 2.1). Isoprene emissions estimated by MEGAN 2.1 accounts for the main processes driving variations in emissions (Guenther *et al.*, 2012). The activity factor for isoprene (γ_i) considers the emission response to light (γ_P), temperature (γ_T), leaf age (γ_A), soil moisture (γ_{SM}), leaf area index (LAI) and CO_2 inhibition (γ_{CO2}) according to Eq. (4):

$$\gamma_i = C_{CE}\, LAI\, \gamma_P \gamma_T \gamma_A \gamma_{SM} \gamma_{CO_2} \quad (4)$$

where C_{CE} is the canopy environment coefficient. For the present study, the canopy environment model of Guenther *et al.* (2006) was used. It has a C_{CE} of 0.57. MEGAN 2.1 was run with variation in light, temperature, and LAI. Based on changes in LAI, the model estimated leaf age of the foliage. Soil moisture and CO_2 inhibition activity factors were assigned a value $\gamma_{SM} = 1$ and $\gamma_{CO2} = 1$, respectively, which assumes no variation in these parameters. More details about the model settings can be obtained in Guenther *et al.* (2012).

Photosynthetic photon flux density (PPFD) and air temperature inputs for all model runs were obtained from the towers K34 (ZF2 site) and INSTANT (ATTO site). LAI inputs were acquired by satellite observations from NASA MODIS during the same period of isoprene flux measurements. The level-4 LAI product is composited every 8 days at 1-km resolution on a sinusoidal grid (MODIS-NASA, 2015). Additionally, by comparison with the default MEGAN 2.1 that uses LAI variation taken from MODIS, here we used LAI

fractionated into different leaf ages, which were modeled based on observations of the cameras installed on top of the towers of both sites.

5. Results

The two experimental sites from where results are presented here – K34 and ATTO - showed seasonal variation in air temperature, Photosynthetic Active Radiation (PAR), and precipitation (Fig. 2). During the dry and the onset of the dry-to-wet transition seasons – from August to October - both sites presented higher values of air temperature and PAR compared to the other seasons. At K34 site, intermittent values of cumulative precipitation estimated by the Tropical Rainfall Measuring Mission (TRMM) was observed for the year 2013, being those values below and above 100 mm $month^{-1}$ from the wet-to-dry transition season (May) to the dry-to-wet transition season (October). At ATTO site, mean cumulative precipitation (2012-2015) was below 100 mm $month^{-1}$ between transition seasons of wet-to-dry and dry-to-wet (July-November), but error bars were below 100 mm $month^{-1}$ only in August and September.

Similarly to air temperature and PAR, OMI satellite-derived isoprene flux presented higher values during the dry and the dry-to-wet transition seasons for both sites (Fig. 3). Mean fluxes estimated for the K34 site (from 2005 to 2014, and for 2013) were around a factor of two of mean fluxes estimated for the ATTO site domain (from 2012 to 2014), showing a difference in isoprene fluxes between these two sites. However, the 2013-year presented lower satellite-derived isoprene flux compared to 2012 and 2014 for the ATTO site (Fig. S2).

Taking isoprene vertical gradient concentrations of intensive campaigns from November 2012 to October 2015 and turbulence measurements of the ATTO site, ground-based isoprene fluxes were calculated by the Inverse Lagrangian Transport model (ILT). Isoprene fluxes calculated by ILT were seasonally different (Fig. 4). It was observed that

isoprene vertical concentrations increased from wet to dry seasons (Fig. 4c), and this was reflected into the increasing isoprene flux in the same direction (Fig. 4a). Isoprene fluxes from all the wet and the wet-to-dry seasons were negative, revealing deposition; the dry and the dry-to-wet transition seasons presented positive isoprene fluxes (emission). The main source of isoprene was the upper canopy (~25 m), where there is a peak of leaf area density (Fig. 4b) and high availability of light and high temperature. Additionally, REA measurements were carried out in one intensive campaign at ATTO site in 2015. REA isoprene flux results showed that the average of emissions in November 2015 – *El-niño* year - was a factor of three lower than emissions in November 2012 (ILT).

For the K34 site, isoprene fluxes measured by REA peaked during the dry season and were still high during the beginning of wet season. The lowest emissions were observed during the wet-to-dry transition season (Fig. 5a). Measurements at K34 site were carried out in 2013. By comparing these measurements with those from ATTO site in the same year, it is observed that the K34 site presented higher isoprene fluxes than ATTO site (Fig. 5b). This could be related to differences between both sites, including differences in isoprene emitter distribution and in environmental factors. However, it seems to be a peculiarity of the 2013-year, because satellite-derived isoprene fluxes were also lower than other years at the ATTO site (Fig. S2), and fluxes (mean and one standard deviation) are in the same range when comparing measurements during the dry and the dry-to-wet transition seasons of K34 site in 2013 and of ATTO site in 2012 and 2014.

The forest leaf quantity, shown as Leaf Area Index (LAI), has not presented much variation over the year when the total LAI was accounted (Fig. 6). Then, total LAI was fractionated into three different leaf ages – young LAI, mature LAI, and old LAI – in order to verify the seasonality of LAI with different leaf age classes. To understand how those LAI fractions could be related to the isoprene seasonality, fluxes of this compound of both sites

were compared to the LAI age fractions estimated for all over the year (Fig. 6). The highest emissions were observed when the number of trees with mature leaves (mature LAI) was increasing for both sites. Considering seasonal changes in PAR, temperature, and mature LAI, this last was the most correlated factor and explained up to 59% of seasonal isoprene emissions (Table 2).

In order to better represent and model the role that leaf phenology plays on isoprene emissions, two different LAI datasets were used to input the leaf age algorithm in the MEGAN 2.1 (Fig. 7): first, LAI provided by the MODIS (MODIS-LAI, default); and secondly, LAI fractionated into the different leaf ages estimated on basis of camera observations in the field (CAMERA-LAI). Both runs also used datasets of PPFD and air temperature measured in the two sites.

Although MEGAN 2.1 estimates presented similarities with isoprene fluxes observed in the sites, in terms of magnitude this happened only for few months (Fig. 7). Also, MEGAN 2.1 did not catch the same seasonal behavior observed in the fields. Regressions between averages of observations and MEGAN 2.1 estimates were not statistically significant: for the K34 site - REA observations versus MEGAN 2.1 (MODIS-LAI) r^2= 0.24 and REA observations versus MEGAN 2.1 (CAMERA-LAI) r^2= 0.19; for the ATTO site – ILT versus MEGAN 2.1 (MODIS-LAI) r^2= 0.04 and ILT observations versus MEGAN 2.1 (CAMERA-LAI) r^2= 0.04. MEGAN 2.1 estimates with input of LAI observed *in situ* only showed a reduction in isoprene flux magnitudes, and it kept the same curve behavior observed in the estimates made with the default MEGAN 2.1 for both sites.

6. Discussion

This study addressed three main questions about the seasonality of isoprene fluxes in central Amazonia and also indicates possible limitations in our current understanding related to these questions.

What is the seasonal pattern of isoprene fluxes of two primary rainforest sites in central Amazonia?

Our results confirm that isoprene emissions are lower during the wet season than the dry season in Amazonia, as suggested by previous studies (Barkley *et al.*, 2009; Alves *et al.*, 2016). But, here we present high isoprene emissions for both sites during the dry and the dry-to-wet transition seasons and deposition during the wet and the wet-to-dry transition seasons in the ATTO site for two consecutively years, which is so far not shown and not considered as a significant process involving seasonal isoprene fluxes.

The way how trace gases are vertically distributed within- and above-canopy depends on the source magnitude of emissions, sink-source distribution, and turbulence characteristics (Fuentes *et al.*, 2016). Isoprene exchanges between the forest and the atmosphere result from the equivalent partial pressure gradient, which is a combination between turbulence and diffusion, multiplied by the transfer velocity; thus, isoprene deposition can be observed when above-canopy partial air pressure is higher than the below-canopy one (Spielmann *et al.*, 2016). Here, isoprene deposition only observed during the wet and the wet-to-dry transition seasons can be explained by the fact that isoprene concentrations were higher above canopy, and it was not observed a source of isoprene within canopy as compared to the dry and the dry-to-wet transition seasons. But, what are the possible reasons and processes involved to have isoprene deposition only during the wet and the wet-to-dry transition seasons?

As isoprene deposition was not observed before in Amazonia, the possible reasons for these results are based on hypothesis that need to be tested. One hypothesis could be that the tower surrounding area has higher emissions than the tower local area. During the dry season, light and temperature are high and this would stimulate emissions in the whole area, giving a net isoprene emission that is observed in this study. However, during the wet and wet-to-dry seasons those environmental factors are not at their highest and, if the tower local area has more non-emitters or weak-emitters compared to the tower surrounding area, local emissions could be low and advection could act as one important process to contribute for local net isoprene deposition.

Another hypothesis could be the soil isoprene consumption. At least part of the isoprene deposition could be resultant of soil being a sink for isoprene (Cleveland & Yavitt, 1997; Pegoraro *et al.*, 2005, 2006, Gray *et al.*, 2014, 2015; Spielmann *et al.*, 2016). Pegoraro *et al.* (2006) have shown that soil moisture influences on isoprene soil consumption in a tropical rainforest mesocosm. They found that when soil was wet, soil isoprene uptake increased rapidly with the increasing of atmospheric isoprene concentration, whereas during dry conditions isoprene soil consumption showed a slower response. Perhaps, the isoprene deposition observed here is resultant of the increasing isoprene soil uptake due to the potential increasing microbial activity during the wetter periods, indicating that seasonal changes in soil sink capacity could influence the isoprene quantity that is going into the atmosphere in Amazonia.

To understand the pattern of isoprene seasonal fluxes in Amazonia is a difficult task when considered only few ecosystem components. Seasonal variation of light and temperature are thought to primarily drive isoprene seasonal emissions. However, other less general factors might influence the ecosystem isoprene production and consumption. The huge biodiversity in Amazonia provides heterogeneity in species distribution and,

considering that not all species are isoprene emitters, this heterogeneity might cause differences in the strength of isoprene emission between regions, resulting in areas with net emission and areas with net deposition in certain periods of the year.

How seasonal isoprene fluxes can be explained by variations in solar radiation, temperature, and leaf phenology?

Our finding that isoprene emissions are higher during the warmer seasons are consistent with previous findings that tropical tree species are light dependent and stimulated by high temperatures (Harley *et al.*, 2004; Alves *et al.*, 2014; Jardine *et al.*, 2014). But, high emissions were observed until the dry-to-wet transition season, when mean PAR and air temperature were already decreasing. Part of this could be attributed to the inter-annual variability of length and intensity of the dry season in central Amazonia (da Rocha *et al.*, 2009) that causes variation in the months of maximum light and temperature, possibly reflecting to peaks of isoprene emissions during either the dry and the dry-to-wet seasons in different sites and/or different years of measurements (see table 1 of Alves et al., 2016). This inter-annual variability can be seen in the ATTO site that presented isoprene fluxes much lower for November 2015 – *El niño* year – compared to November 2012 (Fig. 5b).

Additionally, there is seasonal variation of biological factors that are related to isoprene emission. Since photosynthesis supplies the carbon to the methyl erythritol phosphate pathway to produce isoprene (Delwiche & Sharkey, 1993; Loreto & Sharkey, 1993; Harley *et al.*, 1999), variation in isoprene emission may arise from seasonal changes in the photosynthetic capacity, which is already reported for central Amazonia (Wu *et al.*, 2016). Wu *et al*. (2016) suggested that leaf demography (canopy leaf age composition) and leaf ontogeny (age-dependent photosynthetic efficiency) are the main reasons for the seasonal

557 variation of the ecosystem photosynthetic capacity. As isoprene emissions are strongly
558 dependent on leaf age and mainly emitted by adult and fully expanded leaves (Alves *et al.*,
559 2014), seasonal changes in the forest leaf age fractions might also influence on the
560 seasonality of isoprene emissions, suggesting more emissions when more mature leaves are
561 available and during high ecosystem photosynthetic capacity efficiency.

562 However, understanding the correlations among light, temperature, leaf phenology
563 (LAI fractionated into age classes), and isoprene is not straightforward. Correlations between
564 ground-based isoprene fluxes and those factors were not strong (Table 2), but the variation of
565 mature LAI correlated better than other factors (K34 site – R^2=59%; ATTO site – R^2=42%),
566 suggesting that the increasing of isoprene emissions could partially follow the increasing of
567 mature leaves (Fig. 6).

568 The weak correlation of seasonal changes between isoprene and light and temperature
569 might be due to seasonal changes in the isoprene dependency to environmental factors and
570 biological factors. Light and temperature peaked at the dry season; mature LAI, Gross
571 Primary Productivity (GPP) and photosynthetic capacity peaked at the wet season (results
572 only for K34 site, Wu *et al.*, 2016); and ground-based isoprene fluxes peaked during the end
573 of the dry and the dry-to-wet transition seasons. This might suggest that isoprene emissions
574 are stimulated by light and high temperatures during the beginning of the dry season, but
575 offset by the lower amount of mature leaves; during the wet season, isoprene emissions could
576 be stimulated by the high quantity of mature leaves, but offset by the lower light availability
577 and lower temperature; and at the end of the dry and at dry-to-wet transition seasons, there is
578 a combination of high light and high temperature with high amount of mature leaves,
579 possibly favoring high isoprene emissions. This is supported by findings of a temperate plant
580 species showing that LAI dependency (changes in leaf age) was the most important factor
581 affecting isoprene emission capacity, but when LAI decreased and senescence started in the

582 end of the summer, PAR and air temperature dependencies of isoprene emission were as high
583 as the period when PAR and air temperature reached their maximum (Brilli *et al.*, 2016).

584 Furthermore, we present a lack of a general correlation between ecosystem seasonal
585 cycles of photosynthetic capacity or GPP and isoprene emissions (Table 2), which is
586 consistent with a previous study that evidenced that isoprene emission rates are decoupled
587 from photosynthesis rates at high temperatures (Foster *et al.*, 2014). In this light, it could be
588 suggested that the strong correlation between GPP and isoprene emission during leaf
589 phenology, as seen for a tree species in Amazonia (Kuhn *et al.*, 2004b), is reduced at
590 conditions of high temperature.

591 As discussed above, separating the effects of changing temperature and light from leaf
592 phenology in canopy isoprene fluxes could allow for a more accurate quantification and for
593 better understanding of seasonal isoprene flux. Here, we indicate that leaf phenology plays an
594 important role on seasonal variation of isoprene emissions, especially because different leaf
595 ages present different isoprene emission capacity and the proportion of leaf age changes
596 seasonally in Amazonia. However, when air temperature is the highest, isoprene emission
597 could be more stimulated by this factor, even though mature LAI is still not at its maximum.
598 We suggest to future investigation: to verify whether tree species that present a regular
599 seasonal leaf flushing are isoprene emitters and the strength of those emissions by leaf age;
600 and to test whether isoprene emission estimates can be linked to GPP in a way that the
601 decoupling of them due to high temperature could be seen at the ecosystem scale.

602 *How leaf phenology observed in field can help on improving model estimates of isoprene*
603 *seasonal emissions?*

604 Modeling of isoprene emissions from the Amazonian rainforest has been carried out
605 since around thirty years ago. The first models were simplified and were a little optimized

606 with few short field campaigns in Amazonia (see table 1 of Alves *et al.*, 2016). With more
607 been figured out, more driving forces of isoprene emission were accounted for the latest
608 versions of models, as the case of the MEGAN 2.1, which has been improved into a multi-
609 layer canopy model that reproduces light interception and leaf temperature within the canopy,
610 and includes changes in emissions due to leaf age on basis of satellite retrievals of LAI
611 development (Guenther *et al.*, 2012).

612 Results presented here are from MEGAN 2.1 estimates with local observations of
613 PAR, air temperature, and leaf phenology. However, MEGAN 2.1 did not catch the seasonal
614 behavior of isoprene emission observed. This could be related to the effect of leaf aging on
615 isoprene emission capacity. Using the leaf phenology observed in the field as inputs for the
616 leaf age algorithm of MEGAN 2.1, improved estimates of the proportion of leaves in
617 different leaf age categories for the sites, but did not change the relative isoprene emission
618 capacity used for each age class. It has been indicated that MEGAN uncertainties are mostly
619 related to short-term and long-term seasonal and developmental of the isoprene emission
620 capacity (Niinemets *et al.*, 2010). For an Asian tropical forest, isoprene emission capacity can
621 be four times lower than the default value of the MEGAN model (Langford *et al.*, 2010). In
622 addition, satellite retrievals showed significant reductions in isoprene emissions (30-40 % in
623 Amazonia and northern Africa) (Bauwens *et al.*, 2016), suggesting that isoprene emission
624 capacity might not be well represented in the model.

625 To date, there is very little information about isoprene emission capacity for different
626 leaf ages of Amazonian plant species (Kuhn *et al.*, 2004b; Alves *et al.*, 2014). The scarcity of
627 observational studies in the field, joined with the huge biodiversity and heterogeneity of the
628 Amazonian ecosystems, creates a challenge to optimize the isoprene emission capacity
629 parameterization in the MEGAN and other models. Therefore, introducing local seasonal
630 changes of canopy leaf age fractions in the model is a great advantage, but to better represent

631 the effects of leaf phenology on ecosystem isoprene emissions, seasonal variations in
632 isoprene emission capacity also need to be known.

633 *Possible limitations*

634 This study intended to correlate as much as data were available and it related variables
635 of different scales and approaches. However, here we have limitations that need to be
636 considered. One is the uncertainty related to the methods of ground-based isoprene flux
637 measurements. For the K34 site, the uncertainties of the REA flux measurements ranged from
638 27.1% to 44.9% (more details in section 3 of Supporting Information). For the ATTO site,
639 isoprene flux uncertainty is estimated to be up to 36 %. These uncertainties are similar to
640 what was found in a study carried out in another site at central Amazonia (+/- 30% of
641 uncertainty) (Karl *et al.*, 2009, 2010). Isoprene flux errors are mainly related to errors in
642 measurements of turbulence and isoprene concentrations. However, this study shows the
643 largest dataset of seasonal isoprene fluxes in Amazonia presented to date and, except for the
644 isoprene deposition, results presented here are somehow similar to previous investigations,
645 when results of the same seasons are compared (see table 1 of Alves *et al.*, 2016).

646 The other possible limitation is with respect to the uncertainties in MEGAN estimates
647 of both sites. It has been indicated that models tend to agree with observations within ~30%
648 for canopy scale studies with site-specific parameters (Lamb *et al.*, 1996). Here, we
649 suggested that the unknown isoprene emission capacity for the different leaf age classes
650 found in the forest may be the main reason why MEGAN 2.1 did not represent well the
651 observed seasonality of isoprene fluxes. But, these model uncertainties do not arise simply
652 because of a lack of isoprene leaf-level measurements, but also of: canopy structure and light
653 interception, including within-canopy variation in leaf functional traits (Niinemets, 2016); the
654 physical processes by which isoprene is transported within and above the forest canopy;

deposition; and chemical reactions that can take place within the canopy (Misztal *et al.*, 2011).

Therefore, most of the limitations are related to the lack of measurements. More measurements are very needed to improve our understanding of the mechanisms behind the processes involved in the seasonality of emission and deposition of isoprene in Amazonia, which will improve surface emission and deposition models that will subsequently lead to a better predictive capability of atmospheric chemistry, biogeochemical cycles, and climate.

Acknowledgements

The authors thank the National Institute for Amazonian Research (INPA) and the Max Planck Society for continuous support. We acknowledge the support by the Large Program of Biosphere-Atmosphere Interactions (LBA) and by the ATTO project (German Federal Ministry of Education and Research, BMBF funds 01LB1001A; Brazilian Ministério da Ciência, Tecnologia e Inovação FINEP/MCTI contract 01.11.01248.00), UEA and FAPEAM, LBA/INPA, and SDS/CEUC/RDS-Uatumã. We acknowledge the micrometeorological group of INPA/LBA for their collaboration concerning the meteorological parameters. We acknowledge Kolby Jardine for providing gas standard to calibrate the analytical system. We would like to acknowledge Stefan Wolff for the construction, support and maintenance of the inlet system at the ATTO site. This paper contains results of research conducted under the Technical/Scientific Cooperation Agreement between the National Institute for Amazonian Research, the State University of Amazonas, and the Max-Planck-Gesellschaft e.V.; the opinions expressed are the entire responsibility of the authors and not of the participating institutions.

References

Adams DK, Fernandes RMS, Maia JMF (2011) GNSS Precipitable Water Vapor from an Amazonian Rain Forest Flux Tower. *Journal of Atmospheric and Oceanic Technology*, **28**, 1192–1198.

Adams DK, Gutman SI, Holub KL, Pereira DS (2013) GNSS observations of deep convective time scales in the Amazon. *Geophysical Research Letters*, **40**, 2818–2823.

Alves EG, Harley P, Gonçalves JFDC, Eduardo C, Jardine K (2014) Effects of light and temperature on isoprene emission at different leaf developmental stages of Eschweilera coriacea in central Amazon. *Acta Amazonica*, **44**, 9–18.

Alves EG, Jardine K, Tota J et al. (2016) Seasonality of isoprenoid emissions from a primary rainforest in central Amazonia. *Atmospheric Chemistry and Physics*, **16**, 3903–3925.

Andreae MO, Artaxo P, Brandao C et al. (2002) Biogeochemical cycling of carbon, water,

691 energy, trace gases, and aerosols in Amazonia: The LBA-EUSTACH experiments.
692 *Journal of Geophysical Research-Atmospheres*, **107**.

693 Andreae MO, Acevedo OC, Araùjo A et al. (2015) The Amazon Tall Tower Observatory
694 (ATTO): overview of pilot measurements on ecosystem ecology, meteorology, trace
695 gases, and aerosols. *Atmospheric Chemistry and Physics*, **15**, 10723–10776.

696 de Araújo a. C, Dolman a. J, Waterloo MJ et al. (2010) The spatial variability of CO2
697 storage and the interpretation of eddy covariance fluxes in central Amazonia.
698 *Agricultural and Forest Meteorology*, **150**, 226–237.

699 Arneth A, Monson RK, Schurgers G, Niinemets U, Palmer PI (2008) Why are estimates of
700 global terrestrial isoprene emissions so similar (and why is this not so for
701 monoterpenes)? *Atmospheric Chemistry and Physics*, **8**, 4605–4620.

702 Arnts RR, Mowry FL, Hampton GA (2013) A high-frequency response relaxed eddy
703 accumulation flux measurement system for sampling short-lived biogenic volatile
704 organic compounds. *Journal of Geophysical Research Atmospheres*, **118**, 4860–4873.

705 Barkley MP, Palmer PI, Kuhn U et al. (2008) Net ecosystem fluxes of isoprene over tropical
706 South America inferred from Global Ozone Monitoring Experiment (GOME)
707 observations of HCHO columns. *Journal of Geophysical Research*, **113**, D20304.

708 Barkley MP, Palmer PI, De Smedt I, Karl T, Guenther A, Van Roozendael M (2009)
709 Regulated large-scale annual shutdown of Amazonian isoprene emissions? *Geophysical*
710 *Research Letters*, **36**, L04803.

711 Barkley MP, Smedt I De, Van Roozendael M et al. (2013) Top-down isoprene emissions over
712 tropical South America inferred from SCIAMACHY and OMI formaldehyde columns.
713 *Journal of Geophysical Research: Atmospheres*, **118**, 6849–6868.

714 Bauwens M, Stavrakou T, M??ller JF et al. (2016) Nine years of global hydrocarbon
715 emissions based on source inversion of OMI formaldehyde observations. *Atmospheric*
716 *Chemistry and Physics*, **16**, 10133–10158.

717 Bowling DR, Turnipseed a. a., Delany a. C, Baldocchi DD, Greenberg JP, Monson RK
718 (1998) The use of relaxed eddy accumulation to measure biosphere-atmosphere
719 exchange of isoprene and other biological trace gases. *Oecologia*, **116**, 306–315.

720 Brilli F, Gioli B, Fares S et al. (2016) Rapid leaf development drives the seasonal pattern of
721 volatile organic compound (VOC) fluxes in a "coppiced" bioenergy poplar plantation.
722 *Plant, Cell and Environment*, **39**, 539–555.

723 Claeys M, Graham B, Vas G et al. (2004) Formation of secondary organic aerosols through
724 photooxidation of isoprene. *Science*, **303**, 1173–1176.

725 Cleveland CC, Yavitt JB (1997) Consumption of atmospheric isoprene in soil. *Geophysical*
726 *Research Letters*, **24**, 2379–2382.

727 Cuartas LA, Tomasella J, Nobre AD et al. (2012) Distributed hydrological modeling of a
728 micro-scale rainforest watershed in Amazonia: Model evaluation and advances in
729 calibration using the new HAND terrain model. *Journal of Hydrology*, **462**–**463**, 15–27.

730 DELWICHE CF, SHARKEY TD (1993) Rapid appearance of 13C in biogenic isoprene when

731 13CO2 is fed to intact leaves. *Plant, Cell & Environment*, **16**, 587–591.

732 Foster PN, Prentice IC, Morfopoulos C, Siddall M, Van Weele M (2014) Isoprene emissions
733 track the seasonal cycle of canopy temperature, not primary production: Evidence from
734 remote sensing. *Biogeosciences*, **11**, 3437–3451.

735 Fuentes JD, Chamecki M, Nascimento dos Santos RM et al. (2016) Linking Meteorology,
736 Turbulence, and Air Chemistry in the Amazon Rain Forest. *Bulletin of the American*
737 *Meteorological Society*, **97**, 2329–2342.

738 Goldstein AH, Galbally IE (2007) Known and Unexplored Organic Constituents in the
739 Earth's Atmosphere. *Environmental Science & Technology*, **41**, 1514–1521.

740 Gray CM, Monson RK, Fierer N (2014) Biotic and abiotic controls on biogenic volatile
741 organic compound fluxes from a subalpine forest floor. *Journal of Geophysical*
742 *Research: Biogeosciences*, **119**, 547–556.

743 Gray CM, Helmig D, Fierer N (2015) Bacteria and fungi associated with isoprene
744 consumption in soil. *Elementa: Science of the Anthropocene*, **3**, 53.

745 Guenther a., Karl T, Harley P, Wiedinmyer C, Palmer PI, Geron C (2006) Estimates of
746 global terrestrial isoprene emissions using MEGAN (Model of Emissions of Gases and
747 Aerosols from Nature). *Atmospheric Chemistry and Physics*, **6**, 3181–3210.

748 Guenther a. B, Jiang X, Heald CL, Sakulyanontvittaya T, Duhl T, Emmons LK, Wang X
749 (2012) The Model of Emissions of Gases and Aerosols from Nature version 2.1
750 (MEGAN2.1): an extended and updated framework for modeling biogenic emissions.
751 *Geoscientific Model Development*, **5**, 1503–1560.

752 Harley P, Monson R, Lerdau M (1999) Ecological and evolutionary aspects of isoprene
753 emission from plants. *Oecologia*, **118**, 109–123.

754 Harley P, Vasconcellos P, Vierling L et al. (2004) Variation in potential for isoprene
755 emissions among Neotropical forest sites. *Global Change Biology*, **10**, 630–650.

756 Jardine KJ, Monson RK, Abrell L et al. (2012) Within-plant isoprene oxidation confirmed by
757 direct emissions of oxidation products methyl vinyl ketone and methacrolein. *Global*
758 *Change Biology*, **18**, 973–984.

759 Jardine K, Chambers J, Alves EG et al. (2014) Dynamic balancing of isoprene carbon sources
760 reflects photosynthetic and photorespiratory responses to temperature stress. *Plant*
761 *Physiology*, **166**, 2051–2064.

762 Karl T, Potosnak M, Guenther AB, Clark D, Walker J, Herrick JD, Geron C (2004) Exchange
763 processes of volatile organic compounds above a tropical rain forest: Implications for
764 modeling tropospheric chemistry above dense vegetation. *Journal of Geophysical*
765 *Research*, **109**, D18306.

766 Karl T, Guenther A, Yokelson RJ, Greenberg J, Potosnak M, Blake DR, Artaxo P (2007) The
767 tropical forest and fire emissions experiment: Emission, chemistry, and transport of
768 biogenic volatile organic compounds in the lower atmosphere over Amazonia. *Journal*
769 *of Geophysical Research*, **112**, D18302.

770 Karl T, Guenther a., Turnipseed a., Tyndall G, Artaxo P, Martin S (2009) Rapid formation

771 of isoprene photo-oxidation products observed in Amazonia. *Atmospheric Chemistry*
772 *and Physics*, **9**, 7753–7767.

773 Karl T, Harley P, Emmons L et al. (2010) Efficient Atmospheric Cleansing of Oxidized
774 Organic Trace Gases by Vegetation. *Science*, **330**, 816–819.

775 Kesselmeier J, Kuhn U, Rottenberger S et al. (2002) Concentrations and species composition
776 of atmospheric volatile organic compounds (VOCs) as observed during the wet and dry
777 season in Rondônia (Amazonia). *Journal of Geophysical Research*, **107**, 8053.

778 Kuhn U, Rottenberger S, Biesenthal T et al. (2004a) Seasonal differences in isoprene and
779 light-dependent monoterpene emission by Amazonian tree species. *Global Change*
780 *Biology*, **10**, 663–682.

781 Kuhn U, Rottenberger S, Biesenthal T, Wolf A, Schebeske G, Ciccioli P, Kesselmeier J
782 (2004b) Strong correlation between isoprene emission and gross photosynthetic capacity
783 during leaf phenology of the tropical tree species Hymenaea courbaril with fundamental
784 changes in volatile organic compounds emission composition during early leaf
785 development. *Plant, Cell and Environment*, **27**, 1469–1485.

786 Lamb B, Pierce T, Baldocchi D et al. (1996) Evaluation of forest canopy models for
787 estimating isoprene emissions. *Journal of Geophysical Research*, **101**, 22787–22797.

788 Langford B, Misztal PK, Nemitz E et al. (2010) Fluxes and concentrations of volatile organic
789 compounds from a South-East Asian tropical rainforest. *Atmospheric Chemistry and*
790 *Physics*, **10**, 8391–8412.

791 Laothawornkitkul J, Paul ND, Vickers CE, Possell M, Mullineaux PM, Hewitt CN, Taylor JE
792 (2008) The role of isoprene in insect herbivory. 1141–1142.

793 Laothawornkitkul J, Taylor JE, Paul ND, Hewitt CN (2009) Biogenic volatile organic
794 compounds in the Earth system (vol 183, pg 27, 2009). *New Phytologist*, **184**, 276.

795 Logan BA, Monson RK, Potosnak MJ (2000) Biochemistry and physiology of foliar isoprene
796 production. *Trends in Plant Science*, **5**, 477–481.

797 Lopes AP, Nelson BW, Wu J et al. (2016) Leaf flush drives dry season green-up of the
798 Central Amazon. *Remote Sensing of Environment*, **182**, 90–98.

799 Loreto F, Sharkey TD (1993) On the relationship between isoprene emission and
800 photosynthetic metabolites under different environmental conditions. *Planta*, **189**, 420–
801 424.

802 Loreto F, Velikova V (2001) Isoprene produced by leaves protects the photosynthetic
803 apparatus against ozone damage, quenches ozone products, and reduces lipid
804 peroxidation of cellular membranes. *Plant physiology*, **127**, 1781–7.

805 Loreto F, Mannozzi M, Maris C, Nascetti P, Ferranti F, Pasqualini S (2001) Ozone quenching
806 properties of isoprene and its antioxidant role in leaves. *Plant Physiology*, **126**, 993–
807 1000.

808 Luizao RCC, Luizao FJ, Paiva RQ, Monteiro TF, Sousa LS, Kruijt B (2004) Variation of
809 carbon and nitrogen cycling processes along a topographic gradient in a central
810 Amazonian forest. *Global Change Biology*, **10**, 592–600.

Machado L a. T, Laurent H, Dessay N, Miranda I (2004) Seasonal and diurnal variability of convection over the Amazonia: A comparison of different vegetation types and large scale forcing. *Theoretical and Applied Climatology*, **78**, 61–77.

Malhi Y, Aragão LEOC, Metcalfe DB et al. (2009) Comprehensive assessment of carbon productivity, allocation and storage in three Amazonian forests. *Global Change Biology*, **15**, 1255–1274.

Misztal PK, Nemitz E, Langford B et al. (2011) Direct ecosystem fluxes of volatile organic compounds from oil palms in South-East Asia. *Atmospheric Chemistry and Physics*, **11**, 8995–9017.

MODIS-NASA (2015) No Title. *Leaf Area Index - Fraction of Photosynthetically Active Radiation 8-Day L4 Global 1km*.

Nemitz E, Sutton M a., Gut A, San José R, Husted S, Schjoerring JK (2000) Sources and sinks of ammonia within an oilseed rape canopy. *Agricultural and Forest Meteorology*, **105**, 385–404.

Niinemets Ü (2016) Leaf age dependent changes in within-canopy variation in leaf functional traits: a meta-analysis. *Journal of Plant Research*, **129**, 313–338.

Niinemets U, Monson RK, Arneth A et al. (2010) The leaf-level emission factor of volatile isoprenoids: caveats, model algorithms, response shapes and scaling. *Biogeosciences*, **7**, 1809–1832.

Oliveira AN De, Braule M, Ramos P, Couto LB, Sahdo RM (2008) Composição e diversidade florístico-estrutural de um hectare de floresta densa de terra firme na Amazônia. *Acta Amazonica*, **38**, 627–642.

Pacifico F, Harrison SPP, Jones CDD, Sitch S (2009) Isoprene emissions and climate. *Atmospheric Environment*, **43**, 6121–6135.

Pegoraro E, Abrell L, Van Haren J et al. (2005) The effect of elevated atmospheric CO2 and drought on sources and sinks of isoprene in a temperate and tropical rainforest mesocosm. *Global Change Biology*, **11**, 1234–1246.

Pegoraro E, Rey A, Abrell L, Haren J, Lin G (2006) Drought effect on isoprene production and consumption in Biosphere 2 tropical rainforest. *Global Change Biology*, **12**, 456–469.

Raupach M (1989) Applying Lagrangian Fluid Mechanics to infer scalar source distributions from concentration profiles in plant canopies. *Agricultural and Forest Meteorology*, **47**, 85–108.

Rennó CD, Nobre AD, Cuartas LA, Soares JV, Hodnett MG, Tomasella J, Waterloo MJ (2008) HAND, a new terrain descriptor using SRTM-DEM: Mapping terra-firme rainforest environments in Amazonia. *Remote Sensing of Environment*, **112**, 3469–3481.

da Rocha HR, Manzi AO, Cabral OM et al. (2009) Patterns of water and heat flux across a biome gradient from tropical forest to savanna in Brazil. *Journal of Geophysical Research*, **114**, G00B12.

Rosenstiel TN, Ebbets AL, Khatri WC, Fall R, Monson RK (2004) Induction of poplar leaf

nitrate reductase: A test of extrachloroplastic control of isoprene emission rate. *Plant Biology*, **6**, 12–21.

Sanadze GA (2004) Biogenic isoprene (a review). *Russian Journal of Plant Physiology*, **51**, 729–741.

Sharkey TD, Singsaas EL (1995) Why plants emit isoprene. *Nature*, **374**, 769–769.

Spielmann FM, Langebner S, Ghirardo A, Hansel A, Schnitzler JP, Wohlfahrt G (2016) Isoprene and ??-pinene deposition to grassland mesocosms. *Plant and Soil*, 1–10.

Stavrakou T, Müller J-F, De Smedt I, Van Roozendael M, van der Werf GR, Giglio L, Guenther a. (2009) Global emissions of non-methane hydrocarbons deduced from SCIAMACHY formaldehyde columns through 2003–2006. *Atmospheric Chemistry and Physics Discussions*, **9**, 4609–4651.

Stavrakou T, Müller J-F, Bauwens M et al. (2014) Isoprene emissions over Asia 1979–2012: impact of climate and land-use changes. *Atmospheric Chemistry and Physics*, **14**, 4587–4605.

Stavrakou T, Müller J-F, Bauwens M et al. (2015) How consistent are top-down hydrocarbon emissions based on formaldehyde observations from GOME-2 and OMI? *Atmospheric Chemistry and Physics Discussions*, **15**, 12007–12067.

Terry GM, Stokes NJ, Hewitt CN, Mansfield T a (1995) Exposure to isoprene promotes flowering in plants. *Journal of Experimental Botany*, **46**, 1629–1631.

Tóta J, Fitzjarrald DR, da Silva Dias M a F (2012) Amazon rainforest exchange of carbon and subcanopy air flow: Manaus LBA site--a complex terrain condition. *TheScientificWorldJournal*, **2012**, 165067.

Vickers CE, Possell M, Cojocariu CI et al. (2009) Isoprene synthesis protects transgenic tobacco plants from oxidative stress. *Plant, cell & environment*, **32**, 520–31.

Wu J, Albert LP, Lopes AP et al. (2016) Leaf development and demography explain photosynthetic seasonality in Amazon evergreen forests. *Science*, **351**.

Yáñez-Serrano AM, Nölscher a C, Williams J et al. (2015) Diel and seasonal changes of biogenic volatile organic compounds within and above an Amazonian rainforest. *Atmos. Chem. Phys.*, **15**, 3359–3378.

887 **Tables**

888 **Table 1: Intensive campaigns at the ATTO site**

Year	Month	Days	Season
2012	November	from 18 to 29	dry-to-wet transition season
2013	February	from 20 to 28	wet season
2013	March	from 1 to 06	wet season
2013	June	from 09 to 15	wet-to-dry transition season
2013	September	from 20 to 29	dry season
2014	February	from 25 to 28	wet season
2014	March	from 1 to 13	wet season
2014	August	from 14 to 29	dry season
2015	October	from 10 to 29	dry season – *El niño* year

889

890 **Table 2: Correlation coefficient, R^2, between ground-based isoprene flux and**
891 **environmental and biological factors**

Ground-based isoprene flux	**PAR**	**Temperature**	**mature LAI**	**Photosynthetic capacity***	**GPP***
K34 site	0.001[a]	0.12[a]	0.59[b]	0.49[a]	0.36[a]
ATTO site	0.22[a]	0.35[a]	0.42[b]		

892 * Data from Wu *et al.* (2016)
893 [a] not statistically significant ($P > 0.05$)
894 [b] statistically significant ($P < 0.05$)
895

896

897

898

899

Figures

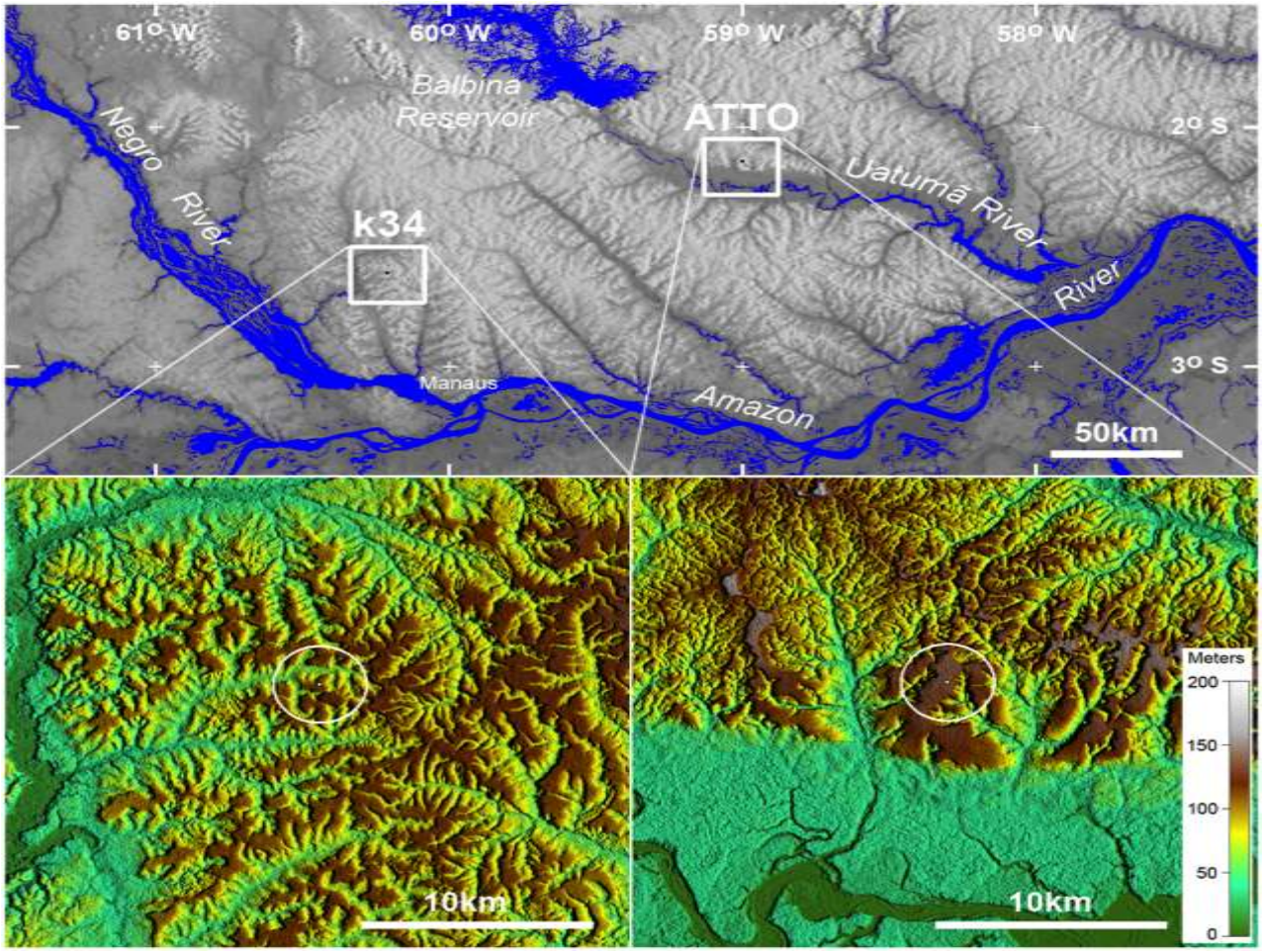

Fig. 1: Location of the two experimental sites in central Amazonia – K34 tower and ATTO (INSTANT tower). Hill-shaded digital elevation data used as background topography is from the Shuttle Radar Topography Mission, with resolutions of ~900m (top panel) and ~30m (lower panels). White rings indicate two km radius around each flux tower. Elevation scale for lower panels is "meters above sea level".

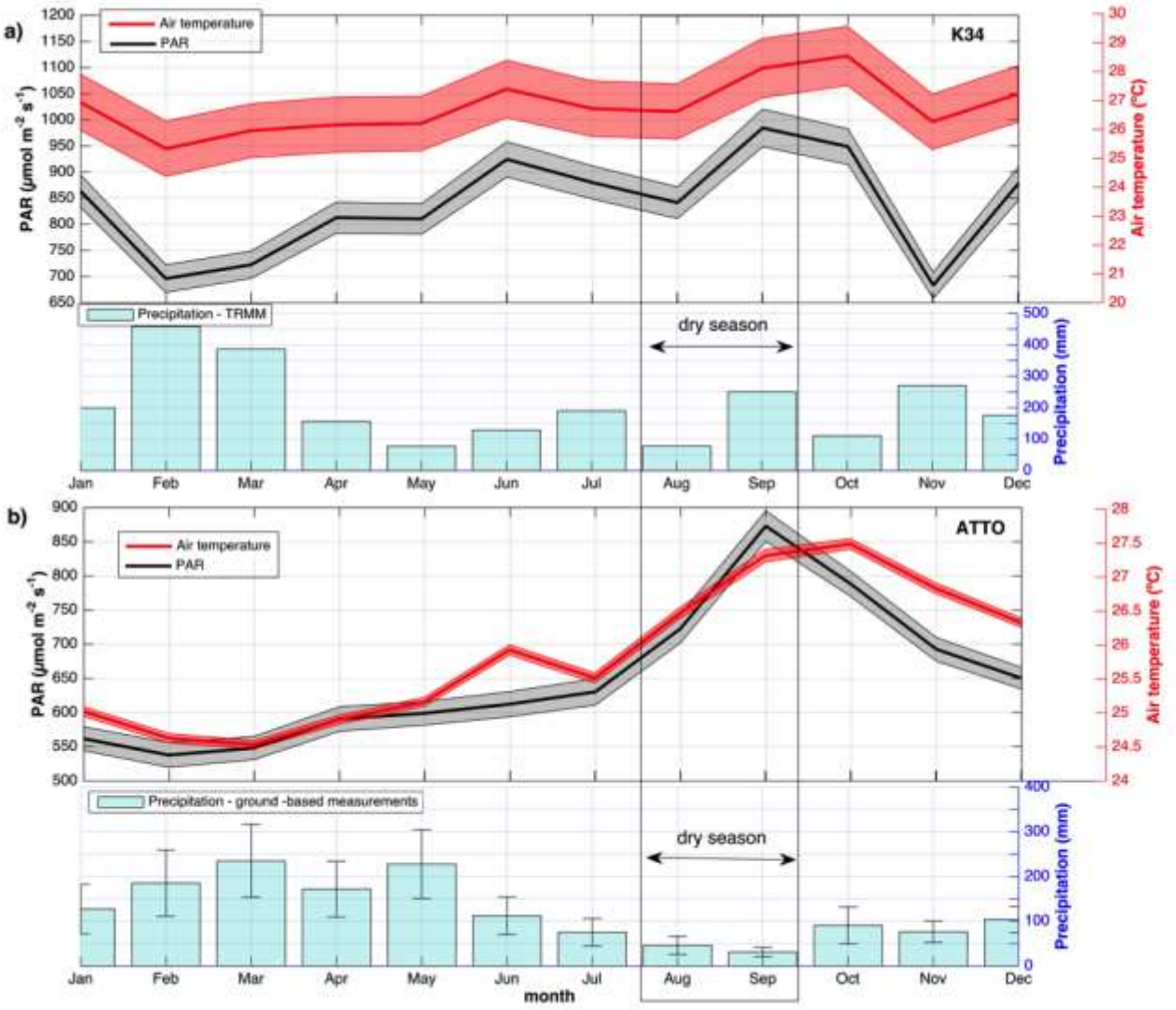

908
909 **Fig. 2**: Monthly averages of Photosynthetic Active Radiation (PAR) and air
910 temperature, measured every 30 minutes, and cumulative precipitation given by the
911 Tropical Rainfall Measuring Mission (TRMM) for the K34 tower site in 2013 (a).
912 Monthly averages of PAR, air temperature and cumulative precipitation measured
913 every minute at the INSTANT tower in the ATTO site from 2012 to 2015 (b).
914 Shading in PAR and in air temperature, and error bars in precipitation represent one
915 standard error of the mean.
916
917

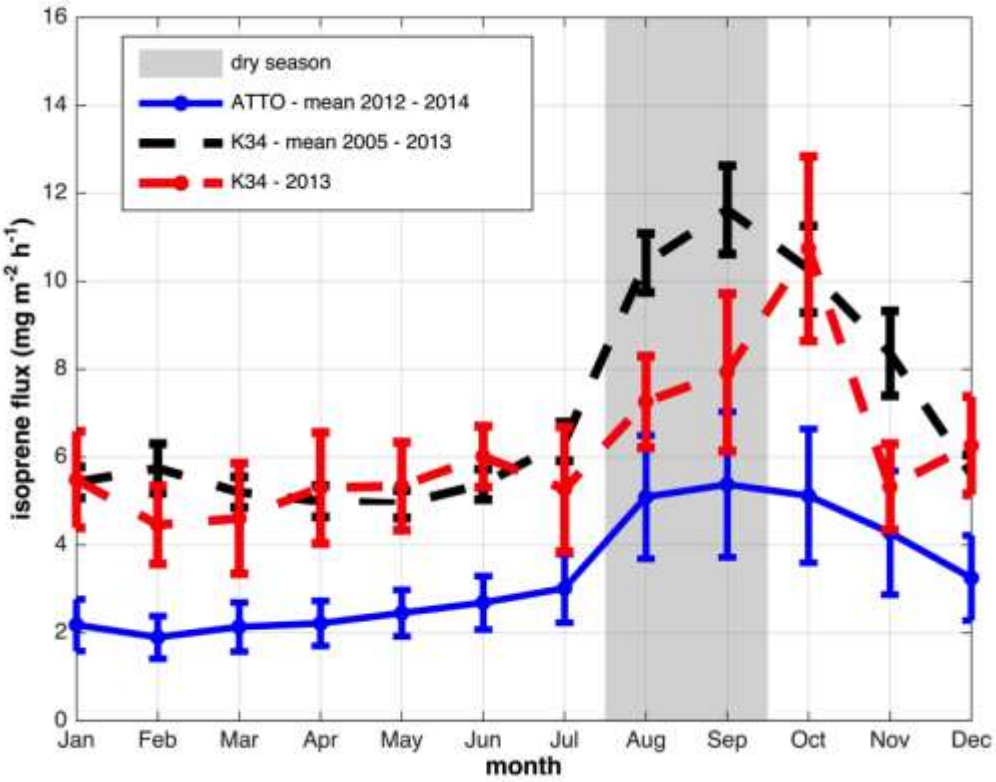

Fig. 3: OMI satellite-derived isoprene flux in a resolution of 0.5º centered on both sites - K34 tower and ATTO. Monthly averages of isoprene flux were scaled to 10-14h, local time. Error bars represent one standard error of the mean. Shading indicates the dry season.

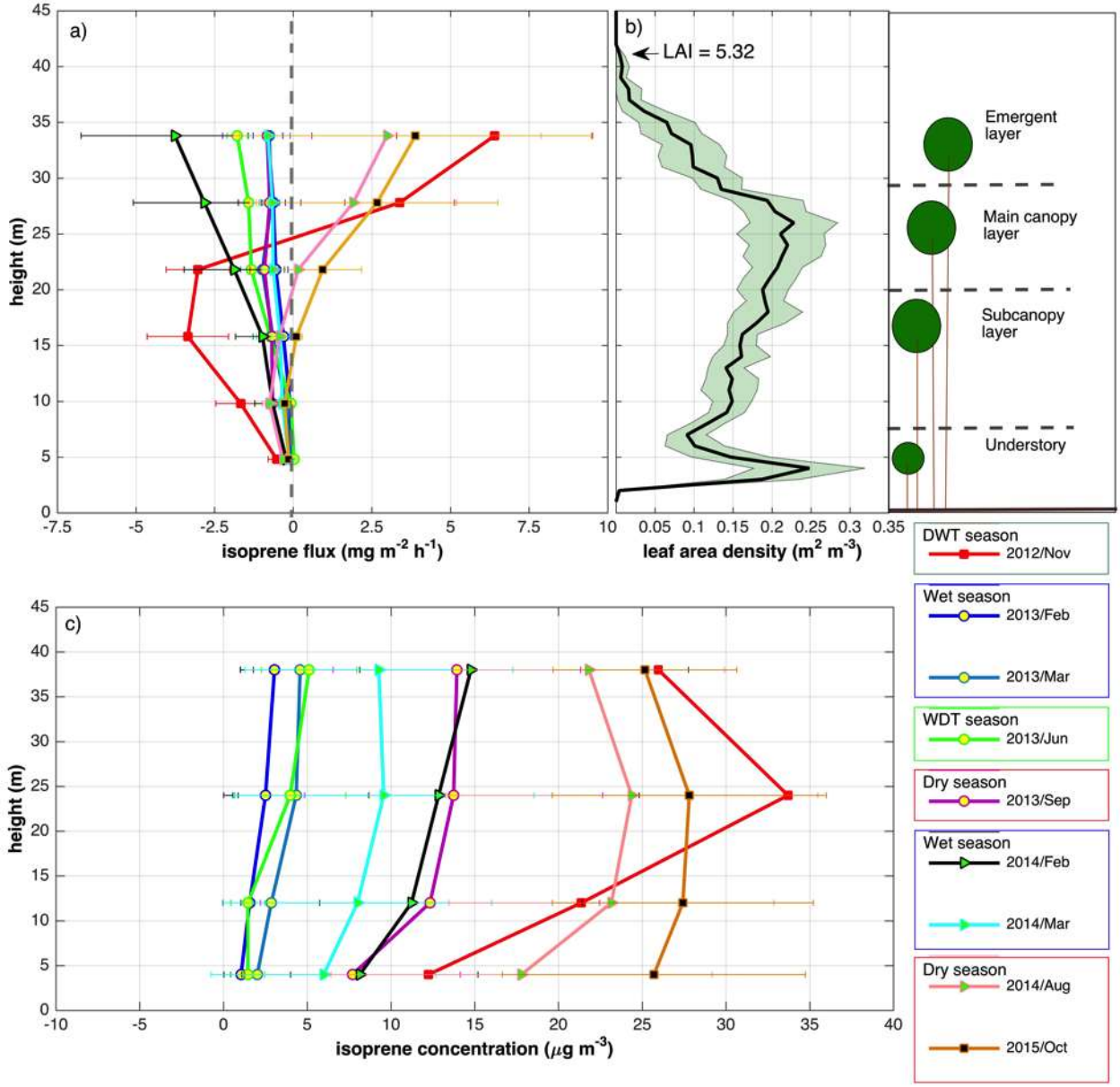

Fig. 4: Isoprene flux profiles for all campaigns; fluxes are presented as mean and one standard deviation (a). Canopy profile of leaf area density (LAD) measured around the INSTANT tower in October 2015 with a ground Light Detection and Ranging sensor (LIDAR) (see section 2 of SI for more information about data acquisition). LAD profiles are presented as mean and confidence interval of 95% (b). Isoprene concentration profiles for all campaigns; concentrations are presented as mean and one standard deviation (c).

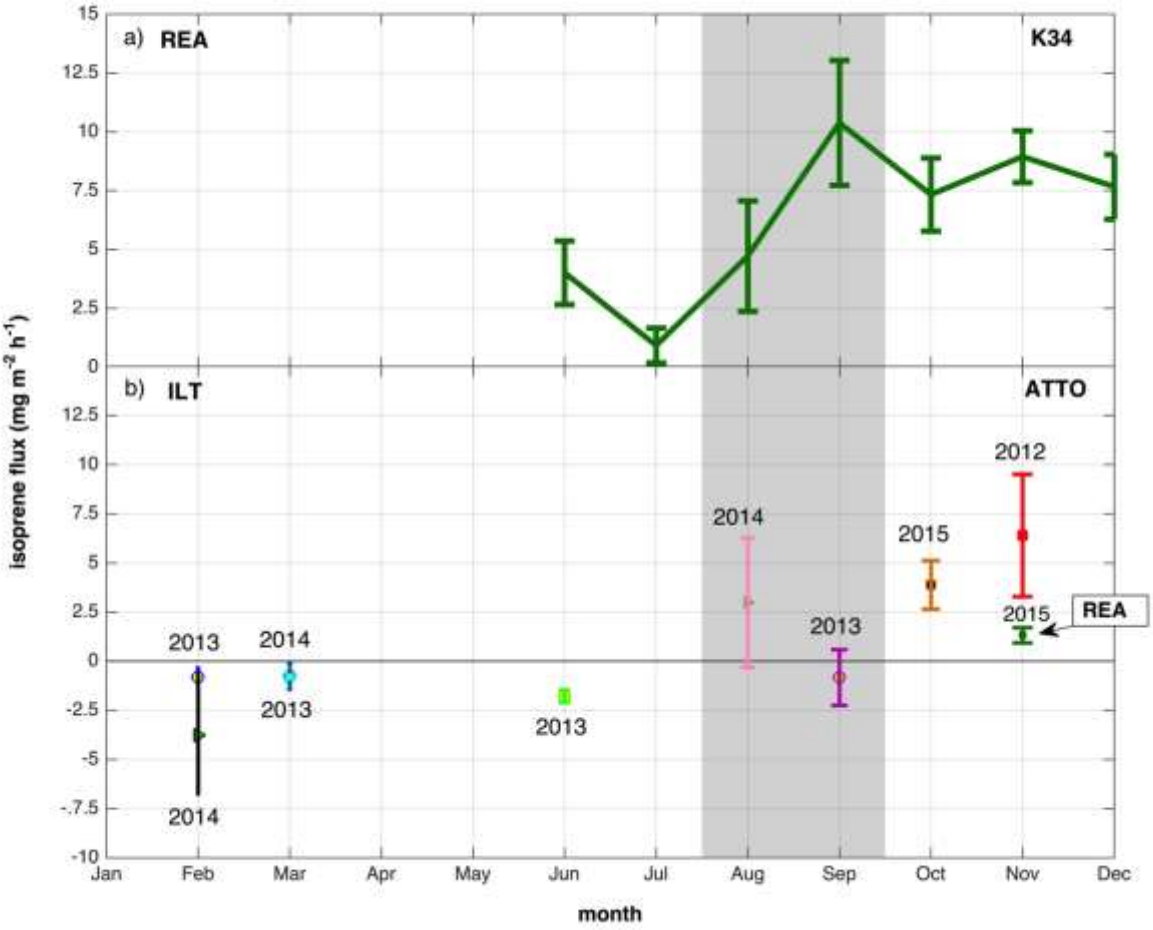

933
934 **Fig. 5:** Isoprene flux measured with the REA system at the K34 tower site in 2013 (a).
935 Isoprene flux calculated by the ILT in intensive campaigns from 2012 to 2015, and isoprene
936 flux measured with the REA system in one intensive campaign in November 2015 at the
937 INSTANT tower – ATTO site (b). Error bars represent one standard deviation of the mean.
938 Shading indicates the dry season.
939

940

941

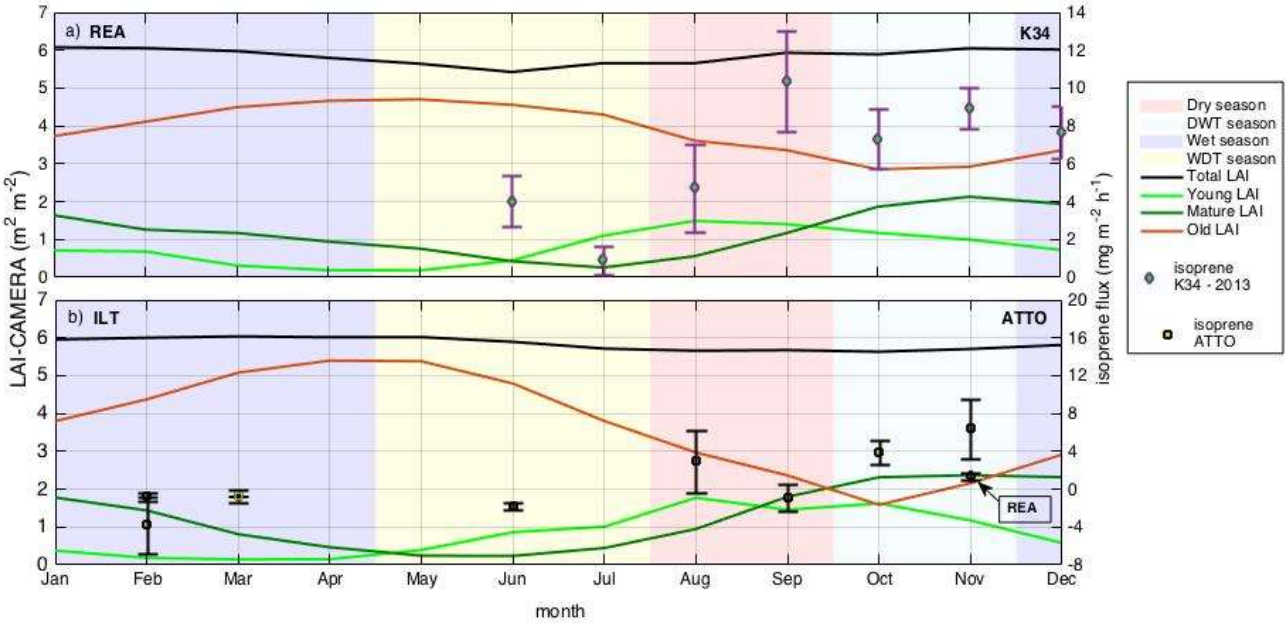

Fig. 6: CAMERA-LAI derived for both experimental sites. CAMERA-LAI data are presented in three different leaf age classes: young LAI, mature LAI and old LAI. CAMERA-LAI results are presented for K34 tower site with isoprene fluxes measured with the REA system (a). For the INSTANT tower site (ATTO), CAMERA-LAI, isoprene flux calculated with the ILT for all intensive campaigns, and isoprene flux measured with the REA system (only for November 2015) are presented (b). Error bars represent one standard deviation of the mean. Shadings indicate each season of both sites and are explicit in the legend. DWT season and WDT season stand for the dry-to-wet transition season and the wet-to-dry transition season, respectively.

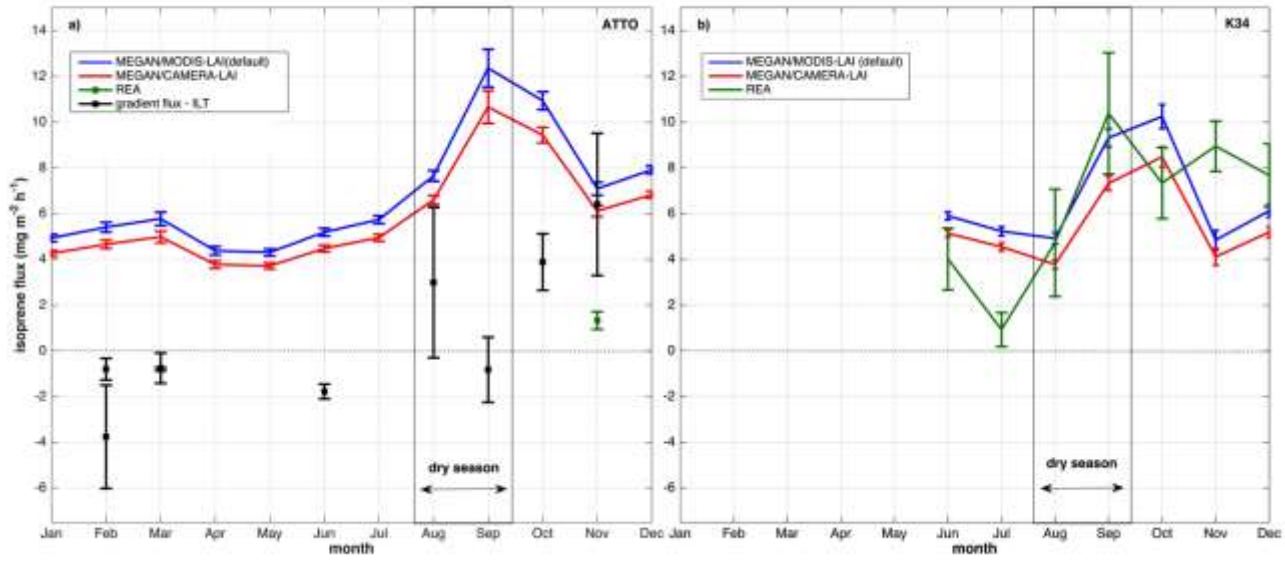

Fig. 7: Isoprene flux observed (ILT and REA) and estimated with MEGAN 2.1 default mode (leaf age algorithm driven by LAI-MODIS) and with MEGAN 2.1 leaf age algorithm driven by CAMERA-LAI, for the ATTO site (a) and k34 site (b).